Magnetic resonance imaging of the liver: apparent diffusion coefficients from multiexponential analysis of b values greater than 50 s/mm2 do not respond to caloric intake despite increased portal-venous blood flow

Pazahr, Shila ; Nanz, Daniel ; Rossi, Cristina ; Chuck, Natalie ; Stenger, Ingo ; Wurnig, Moritz C ; Schick, Fritz ; Boss, Andreas

Abstract: PURPOSE: The purpose of this study was to measure potential changes of the apparent diffusion coefficient (ADC) in diffusion-weighted imaging of the liver before and after caloric challenge in correlation to the induced changes in portal vein flow. MATERIALS AND METHODS: The study was approved by the local ethics committee. Each of 10 healthy volunteers underwent 4 measurements in a 1.5-T whole-body magnetic resonance scanner on 2 different days: a first scan after fasting for at least 8 hours and a second scan 30 minutes after intake of a standardized caloric either a protein- or carbohydrate-rich meal. Diffusion-weighted spin-echo echo-planar magnetic resonance images were acquired at b values of 0, 50, 150, 250, 500, 750, and 1000 s/mm. In addition, portal vein flow was quantified with 2-dimensional phase-contrast imaging (velocity encoding parallel to flow direction, 60 cm/s). Mean ADC values for regions of interest in 3 different slices were measured from b50 to b250 and from b500 to b1000 images. RESULTS: Carbohydrate- and protein-rich food intake both resulted in a substantial increase in the portal vein flow (fasting state, 638.6 ± 202.3 mL/min; after protein intake, 1322 ± 266.8; after carbohydrate intake, 1767 ± 421.6). The signal decay with increasingly strong diffusion weighting (b values from 0 to 1000 s/mm2) exhibited a triexponential characteristic, implying fast, intermediate, and slow-moving water-molecule proton-spin ensembles in the liver parenchyma. Mean ADC for high b values (b500-b1000) after fasting was 0.93 ± 0.09 × 10 mm/s; that after protein intake, 0.93 ± 0.11 × 10; and that after carbohydrate intake, 0.93 ± 0.08 × 10. For intermediate b values (b50-b250), the signal-decay constants were 1.27 ± 0.14 × 10 mm/s, 1.28 ± 0.15 × 10, and 1.31 ± 0.09 × 10, respectively. There was no statistically significant difference between fasting and caloric challenge. CONCLUSIONS: The postprandial increase in portal vein flow is not accompanied by a change of liver parenchymal ADC values. In clinical diffusion imaging, patients may be scanned without prescan food-intake preparations. To minimize interference of perfusion effects, liver-tissue molecular water diffusion should be quantified using high b values (500 s/mm) only.

DOI: https://doi.org/10.1097/RLI.0000000000000005

from multiexponential analysis of b values greater than 50 s/mm2 do not respond to caloric intake despite increased portal-venous blood flow. Investigative Radiology, 49(3):138-146.
DOI: https://doi.org/10.1097/RLI.0000000000000005

Magnetic Resonance Imaging of the Liver

Apparent Diffusion Coefficients From Multiexponential Analysis of b Values Greater Than 50 s/mm^2 Do Not Respond to Caloric Intake Despite Increased Portal-Venous Blood Flow

Shila Pazahr, MD, Daniel Nanz, PhD,* Cristina Rossi, PhD,* Natalie Chuck, MD,* Ingo Stenger, MD,† Moritz C. Wurnig, MD, MSc,* Fritz Schick, MD, PhD,‡ and Andreas Boss, MD, PhD**

Purpose: The purpose of this study was to measure potential changes of the apparent diffusion coefficient (ADC) in diffusion-weighted imaging of the liver before and after caloric challenge in correlation to the induced changes in portal vein flow.

Materials and Methods: The study was approved by the local ethics committee. Each of 10 healthy volunteers underwent 4 measurements in a 1.5-T whole-body magnetic resonance scanner on 2 different days: a first scan after fasting for at least 8 hours and a second scan 30 minutes after intake of a standardized caloric either a protein- or carbohydrate-rich meal. Diffusion-weighted spin-echo echo-planar magnetic resonance images were acquired at b values of 0, 50, 150, 250, 500, 750, and 1000 s/mm^2. In addition, portal vein flow was quantified with 2-dimensional phase-contrast imaging (velocity encoding parallel to flow direction, 60 cm/s). Mean ADC values for regions of interest in 3 different slices were measured from b50 to b250 and from b500 to b1000 images.

Results: Carbohydrate- and protein-rich food intake both resulted in a substantial increase in the portal vein flow (fasting state, 638.6 ± 202.3 mL/min; after protein intake, 1322 ± 266.8; after carbohydrate intake, 1767 ± 421.6). The signal decay with increasingly strong diffusion weighting (b values from 0 to 1000 s/mm2) exhibited a triexponential characteristic, implying fast, intermediate, and slow-moving water-molecule proton-spin ensembles in the liver parenchyma. Mean ADC for high b values (b500-b1000) after fasting was $0.93 \pm 0.09 \times 10^{-3}$ mm^2/s; that after protein intake, $0.93 \pm 0.11 \times 10^{-3}$; and that after carbohydrate intake, $0.93 \pm 0.08 \times 10^{-3}$. For intermediate b values (b50-b250), the signal-decay constants were $1.27 \pm 0.14 \times 10^{-3}$ mm^2/s, $1.28 \pm 0.15 \times 10^{-3}$, and $1.31 \pm 0.09 \times 10^{-3}$, respectively. There was no statistically significant difference between fasting and caloric challenge.

Conclusions: The postprandial increase in portal vein flow is not accompanied by a change of liver parenchymal ADC values. In clinical diffusion imaging, patients may be scanned without prescan food-intake preparations. To minimize interference of perfusion effects, liver-tissue molecular water diffusion should be quantified using high b values (≥500 s/mm^2) only.

Key Words: diffusion-weighted imaging, apparent diffusion coefficient, liver, magnetic resonance imaging

(*Invest Radiol* 2014;49: 138–146)

Received for publication April 3, 2013; and accepted for publication, after revision, August 30, 2013.

From the *Department of Diagnostic and Interventional Radiology, University Hospital of Zürich; †Department of Medicine, Stadtspital Triemli, Zürich, Switzerland; and ‡Section of Experimental Radiology, Department of Diagnostic and Interventional Radiology, University Hospital of Tübingen, Tübingen, Germany.

Conflicts of interest and sources of funding: none declared.

Reprints: Andreas Boss, MD, PhD, Department of Diagnostic and Interventional Radiology, University Hospital of Zurich, Rämistr. 100, 8091 Zürich, Switzerland. E-mail: andreas.boss@usz.ch.

ISSN: 0020-9996/14/4903–0138

Diffusion-weighted imaging (DWI) is increasingly included in clinic liver magnetic resonance imaging (MRI) protocols. Liver DWI was demonstrated to provide important clinical information on the degree of liver fibrosis,[1–4] on the presence and characteristics of benign and malignant liver lesions,[5–8] as well as on treatment response, for example, after transarterial chemoembolization.[9–12]

Up to now, no consensus has been established for the standardization of liver imaging protocols or for the methodology of apparent diffusion coefficient (ADC) map calculations from diffusion-weighted images. The reproducibility of ADC measurements is compromised by intraindividual and interindividual fluctuation, as described in previous studies that found a relatively large test-retest variability of 7% to 14% for the liver parenchyma of healthy volunteers.[13–15] Recent studies described an at least biexponential behavior of the diffusion-weighted signal amplitude decay with increasing b values,[16–18] which is something that has to be taken into account when comparing computed or reported ADC values. Reference ADC values for healthy liver parenchyma are necessary for characterization of diffuse liver pathologies and focal liver lesions.[13,19–21] Furthermore, Annet et al[22] measured a diffusion restriction in the liver of an animal model of liver fibrosis, which was only present in living animals and which was not observed when DWI was performed ex vivo. This result suggests that liver DWI may be influenced by hepatic perfusion. Several studies confirmed these results.[7,23–27] At the same time, it is well known that the portal flow rate increases after food intake.[28–32] Up until now, diffusion-weighted MRI examinations of the liver are done without standardization of the actual nutrition stage. However, it seems conceivable that postprandial changes in the portal blood flow may affect quantitative measurements of water diffusion in the liver parenchyma.

The aim of our study was to measure potential changes of the ADC in DWI of the liver before and after caloric challenge.

MATERIALS AND METHODS

Study Participants

During a 3-month period (November to January 2011), 10 healthy volunteers (6 women and 4 men; mean [SD] age, 23.2 [2.8] years; range, 20–28 years; mean [SD] body mass index, 21.37 [2.6] kg/m^2; range, 17.6–25.3 kg/m^2) were included in this prospective study, which was approved by the local ethics committee. Informed consent was obtained from each volunteer. The volunteers had no history of liver-related diseases. None of the participants used any medication, except oral contraceptives (n = 6).

Magnetic Resonance Scanner

Magnetic resonance studies were performed on a 1.5-T MRI unit (GE Signa; General Electric, Milwaukee, WI) using a 12-channel phased-array flexible body-array coil. All imaging was performed in supine position.

Study Design

Each volunteer underwent 4 examinations with the same imaging protocol in the same magnetic resonance (MR) system on 2 different days. All volunteers were scanned after fasting for at least 8 hours in the first part. In the second part, on the same day, the volunteers were scanned 30 to 35 minutes after intake of a protein drink (commercially purchasable whey protein powder dissolved in water [100% microfiltered whey protein, Lee-Sport; 100 g: 383 kcal, 80-g protein, 16-g branched-chain amino acids, 3.7-g carbohydrates, and 1.7-g fat]). On the second date, the volunteers were first scanned after fasting for at least 8 hours, followed by an MR examination 30 to 35 minutes after an intake of a carbohydrate-rich meal (commercially purchasable durum wheat pasta [Combino,100 g: 357 kcal, 73-g carbohydrates, 12-g protein, 1.2-g fat, and 3-g dietary fiber]). Food intake was adapted to body weight: The volunteers obtained one thirds to one half of their daily energy requirement adapted to their weight, height, and age (400–1100 kcal). The mean (SD) elapsed time between the first 2 examinations and the last 2 examinations was 22 (12) days (median, 27.5; range, 1–35 days).

Imaging Protocol

The imaging protocol started with gradient-echo localizers in all 3 directions for anatomical orientation. An axial and coronal 2-dimensional T2-weighted single-shot fast spin echo sequence was acquired for visualization of the liver morphology and depiction of the portal vein (Figs. 1A, B) (repetition time [TR]/echo time [TE], 1248.9/87.1 milliseconds; bandwidth, 244.14 hertz per pixel; slice thickness, 5 mm; in-plane resolution, 0.82 × 0.82 mm; matrix, 512 × 512 pixel). Portal vein flow was quantified immediately before the DWI sequence as well as 30 and 60 minutes after caloric intake with a single-slice 2-dimensional phase contrast sequence without fat saturation (TR/TE, 11.5/5.5 milliseconds; flip angle, 20 degrees; bandwidth, 61.05 hertz per pixel; slice thickness, 10 mm; in-plane resolution, 0.78 × 0.78 mm; matrix, 512 × 512 pixel; acquisition time, approximately 24 seconds acquired during 1 single breath-hold; 20 cardiac phases; velocity encoding parallel to flow direction, 60 cm/s) in end-expiration using pulse gating (peripheral plethysmograph).[28,33,34] The image plane was selected perpendicular to the portal vein (Figs. 1A, B). For diffusion imaging, a spin-echo echo-planar imaging sequence with the following sequence parameters was applied during shallow breathing: TR/TE, 6300 milliseconds/76.3 milliseconds; parallel imaging acceleration factor, 2; 75% phase partial Fourier, spectral fat suppression, diffusion-sensitizing gradients applied in 3 orthogonal directions separately; b values, 0, 50, 150, 250, 500, 750, and 1000 s/mm^2; slice thickness, 5 mm, receiver bandwidth, 1953 hertz per pixel; 6 averages; in-plane resolution, 1.56 × 1.56 mm; matrix, 256 × 256 pixel; acquisition time, 12 minutes 5 seconds. The participants were previously instructed to breath shallowly during the acquisition of the DWI sequence.

Data Evaluation

Phase Contrast Imaging

From the phase contrast data set, the flow rate of the portal vein was calculated from 20 images reconstructed over a cardiac cycle using a dedicated software (ReportCard 4.0) on a GE (General Electric, Waukesha, WI) workstation. Region of interest (ROI) was defined on the phase image as an area comprising the complete portal vein (Fig. 1C).

Determination of the Diffusion Model

In the DWI data sets, the mean signal intensity was measured using ROIs drawn in the right hepatic lobe (Couinaud liver segments 6 and 7). The ROI was defined on the b0 image and subsequently copied to images acquired with the other b values of the same data set. The signal behavior was mathematically modeled in dependence of the b value with monoexponential, biexponential, and triexponential signal decays obtained by linear least-squares fitting to the normalized logarithm of the signal curve. The accuracy of the diffusion model was quantified through computation of the mean difference between the normalized measurement points and the respective values computed from the mathematical model at the corresponding b values. All evaluations were performed with dedicated routines written in the programming language MATLAB (The Mathworks, Inc, Natick, MA).

Computation of ADC Maps

The ADC maps were calculated using a triexponential diffusion model with a linear fit to logarithmic signal intensities at b = 0 to 50 s/mm^2 (low b values), b = 50 to 250 s/mm^2 (intermediate b values), and b = 500 to 1000 s/mm^2 (high b values) on a pixel-by-pixel basis using a homemade MATLAB computer script (Fig. 2). Similar to the low–b-values scheme, also for all b values greater than 50 s/mm^2, a 2-point calculation of the ADC with b0 was performed to allow for comparison with previously published data. The ROI analysis was performed on the computed ADC maps by the same radiologist (S.P., with more than 3 years of experience in MRI). Free-form ROIs were defined in the parenchyma of the liver segments 6 and 7, avoiding areas affected by cardiac motion-related artifacts as described before.[35–37] Care was taken also to exclude recognizable vessels, bile ducts, and motion artifacts to avoid partial volume effects. The ROI sizes were typically between 20 and 80 mm^2. The ROI measurements were obtained in 3 different slices of each liver: in the level of the portal vein and 3 slices above and below the portal vein (covering 3.0 cm in the craniocaudal direction), respectively.

Phantom Measurement

To validate the DWI sequence and processing methodology, a water phantom was measured using the DWI parameters as described before and applying the identical coil setup as in the volunteer measurements at a room temperature of 22°C. The phantom was filled with an aqueous solution of 1000-mL demineralized water and 770 mg/L of $CuSO4{\cdot}5(H_2O)$. The DWI signal behavior was measured by drawing a rectangular ROI placed within the center of the phantom in 3 different slices of the phantom examination.

Statistical Evaluation

The change of portal flow rate and ADC values caused by food intake was calculated as follows: percentage of change = (postprandial measurement − fasting measurement) × 100/fasting measurement. To avoid cluster bias, the mean of the measured data points for each study participant and examination was calculated; this mean value was used as 1 data point for each person and measurement session in the further statistical evaluation. All final results were described as mean (SD), and the data were descriptively reviewed and statistically tested for normality with the Kolmogorov-Smirnov test. *P* values were calculated by using the Student *t* test for paired samples. A *P* value less than 0.05 was considered significant. In cases where the analysis of variance results indicated that the imaging sessions had no significant effects on the ADC measurements, the coefficient of variation (CV = standard deviation divided by mean and multiplied with 100) was calculated across the imaging sessions for each participant and each ADC map (low, intermediate, and high b values). To estimate the size of a treatment effect that would be detectable in liver DWI, we used the calculated CV.[13] All statistical analyses were performed using commercially available software

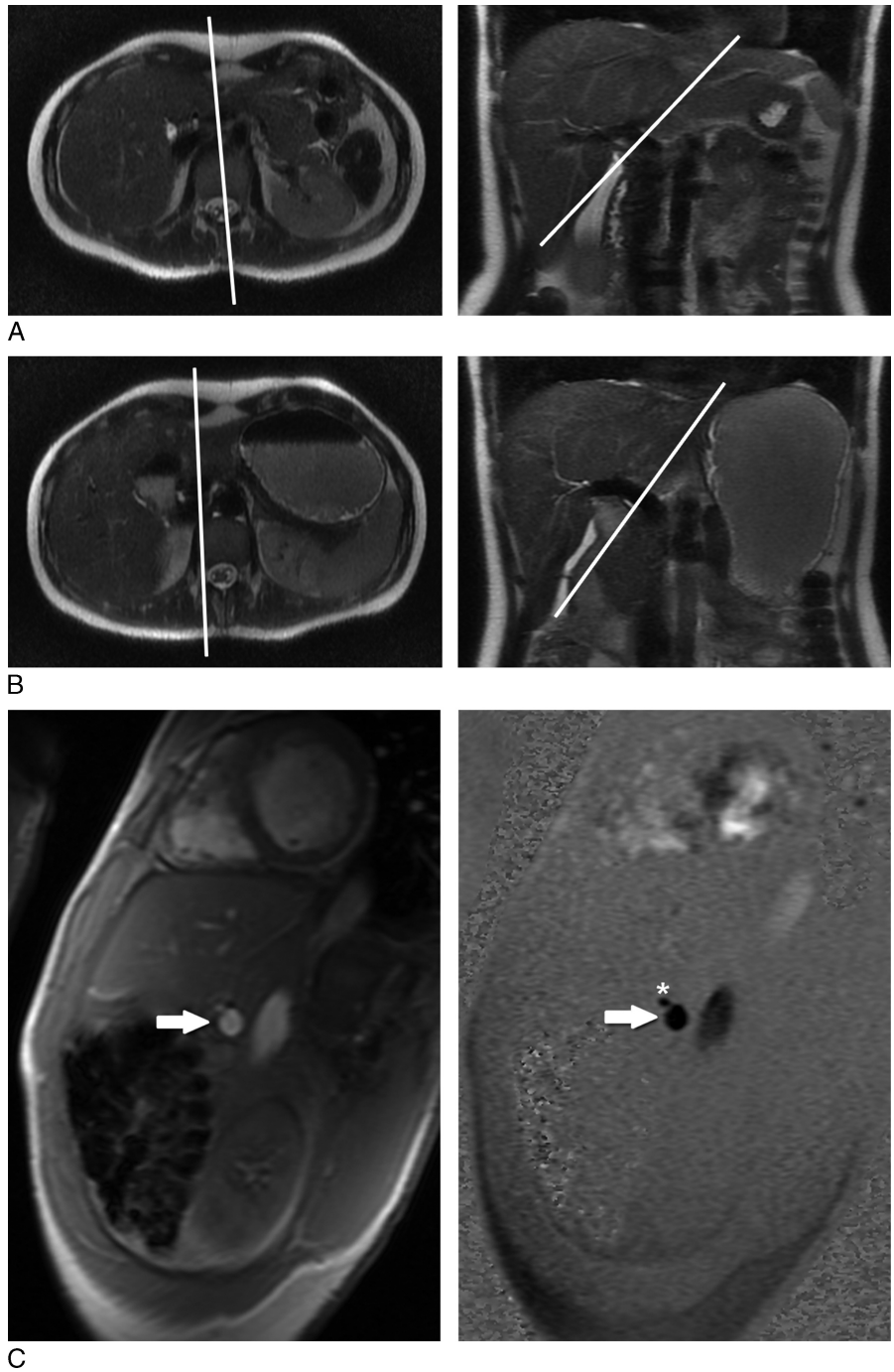

FIGURE 1. Axial and coronal T2-weighted single-shot fast spin echo morphological scout images after fasting for at least 8 hours (A) and after a protein-rich meal with a filled stomach (B). C, Multiphase gradient-echo magnitude (left) and phase-contrast (right) images acquired for measurement of blood volume flow in the portal vein (arrows). The imaging plane in C was oriented perpendicular to the portal-vein long axis (white lines in A and B). C, The common hepatic artery, located above the portal vein, is marked with a star.

(Statistical Package for the Social Sciences, release 17.0; International Business Machines, Armonk, NY).

RESULTS

Portal Vein Flow

The mean (SD) portal blood volume flow after fasting for at least 8 hours was 639 (202) mL/min (range, 302–1033 mL/min; n = 20). The mean (SD) blood volume flow showed a significant increase 30 minutes after the volunteers had a protein- or a carbohydrate-rich meal to 1322 (267) mL/min (range, 938–1689 mL/min; n = 10; $P < 0.0001$) and 1767 (422) mL/min (range, 1178–2420 mL/min; n = 10; $P < 0.0001$), respectively (Fig. 3). The increase in portal volume flow after an intake of carbohydrate-rich food was significantly higher than that after an intake of protein-rich food ($P = 0.014$). The mean (SD) change of portal volumetric flow rate after a meal was 161.4% (97.1%) (range,

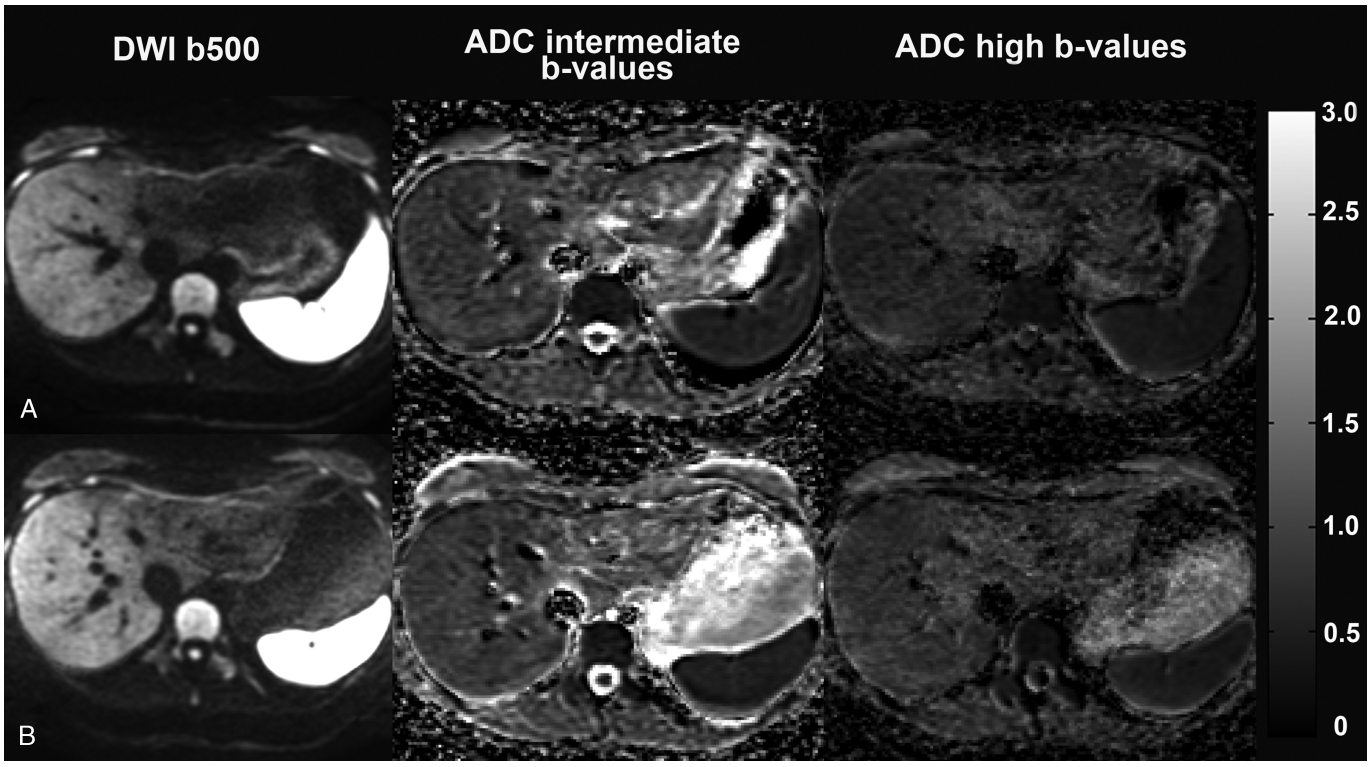

FIGURE 2. Diffusion-weighted imaging for b500 (left column) and the corresponding ADC maps for the same slice calculated pixel-by-pixel for the acquired intermediate b values (b50, b150, and b250 s/mm^2) (center column) as well as for the high b values (b500, b750, and b1000 s/mm^2) (right column) after fasting for at least 8 hours (A) and after a protein-rich meal with a filled stomach (B).

52.6%–352.1%; n = 20). No correlation was found between the portal vein flow and any of the ADC evaluation schemes.

Choice of Diffusion Signal Model

A typical normalized DWI signal curve and the corresponding logarithmic signal curve are depicted in Figure 4. In case of a monoexponential decay, the logarithmic curve should be a straight line with a slope that directly reflects the ADC value. The measured liver-signal decay clearly deviates from a monoexponential mode. For a satisfying modeling of the curve, 3 different components were needed as recently described[18]: a component of fast signal decay (between b = 0 and b = 50 s/mm^2), an intermediate component (b values: 50, 150, and 250 s/mm^2), and a slow component (b, >500 s/mm^2). The accuracy of this triexponential model was demonstrated with the computation of the mean differences between the normalized measurement points and values from the respective exponential model, which was

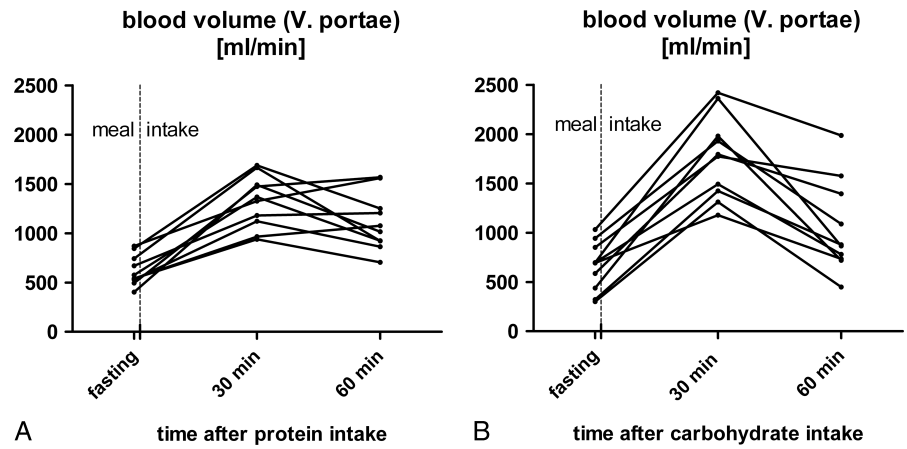

FIGURE 3. Blood volume flow in the portal vein derived from phase-contrast images acquired 30 and 60 minutes after corresponding caloric intake; the graphs represent the changes after a protein-rich meal (A) or after a carbohydrate-rich meal (B) for each of the 10 study participants.

0.5% in intermediate and 0.3% in high b values (Table 1). Each of the 3 phases was fitted separately, instead of applying a sum of the 3 mathematical terms of the 3 phases within 1 fit. The reason for this approach was that nonlinear regression with a similar number of data points and fitting variables is typically mathematically ill-conditioned,[38] resulting in instability of the fit parameters depending on the starting values as observed.

Apparent Diffusion Coefficient Measurements for Low b Values (b0–b50)

Mean measured ADC values after fasting ($4.57 \pm 0.93 \times 10^{-3}$ mm^2/s) were not significantly different from the measurements of the examinations after a protein-rich meal ($4.56 \pm 0.89 \times 10^{-3}$ mm^2/s; $P = 0.17$). Similar results were obtained for the 2 last MR sessions, after fasting and after a carbohydrate-rich meal: $4.78 \pm 0.61 \times 10^{-3}$ mm^2/s and $4.85 \pm 0.94 \times 10^{-3}$ mm^2/s ($P = 0.37$), respectively (Fig. 5). Mean (SD) paired intraindividual differences between fasting and a protein- or carbohydrate-rich food intake was 21.6% (20.7%) and 16.0% (11.3%). The calculated CVs for each participant and each session were 14.1%, 14.4%, 14.0%, and 13.1%, (overall CV for intermediate b values, 13.9%).

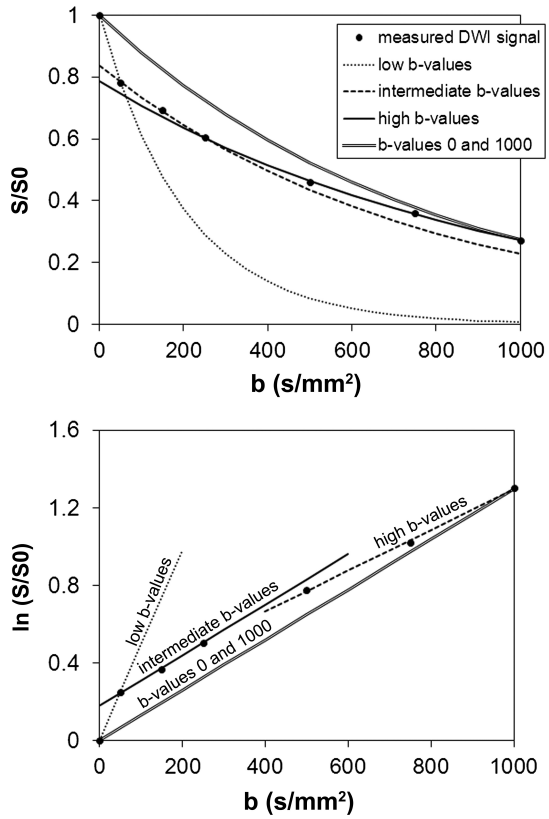

FIGURE 4. A typical DWI signal decay over the range of sampled b values is displayed: black dots indicate normalized DWI measurement points in the upper graph and logarithmic normalized measurement points in the lower graphs. Corresponding fitting curves are represented by different line styles. The slope of each line in the lower graph corresponds to a computed ADC value. Three different phases can be distinguished. The line through the measurement points of the first 2 b values (b0-b50 s/mm^2) shows a steep slope with a corresponding high ADC value (hypothesis: corresponding to microcirculation in small vessels). The second fitting line of the intermediate b values (b50/b150/b250 s/mm^2) exhibits an intermediate slope (hypothesis: representing sinusoidal blood flow). The lowest slope and ADC value are found for high b values (b500, b750, and b1000 s/mm^2), presumably representing pure water diffusion. The thick line corresponds to a monoexponential diffusion model using only b0 and b1000 s/mm^2.

Apparent Diffusion Coefficient Measurements for Intermediate b Values (b50–b250)

The measured mean ADC values for intermediate b values after fasting were $1.26 \pm 0.06 \times 10^{-3}$ mm^2/s. There were no significant differences of the ADC values 30 minutes after intake of a protein-rich meal ($1.28 \pm 0.13 \times 10^{-3}$ mm^2/s; $P = 0.68$). Nearly-identical mean ADC values were obtained in the last 2 sessions for both fasting ($1.28 \pm 0.12 \times 10^{-3}$ mm^2/s) and 30 minutes after intake of a carbohydrate-rich meal ($1.31 \pm 0.06\ 10^{-3}$ mm^2/s) ($P = 0.70$) (Figs. 5, 6). Mean (SD) paired intraindividual differences between fasting and a protein- or carbohydrate-rich food intake was 10.0% (10.6%) and 11.1% (12.4%), respectively. The calculated CVs for each participant and each session were 8.2%, 7.2%, 7.8%, and 5.7% (overall CV for intermediate b values 7.2%); (demonstrated in Table 2).

Apparent Diffusion Coefficient Measurements for High b Values (b500-b1000)

Mean ADC values after fasting and after a protein-rich meal were $0.91 \pm 0.04 \times 10^{-3}$ mm^2/s and $0.93 \pm 0.06 \times 10^{-3}$ mm^2/s, respectively (no statistically significant difference: $P = 0.80$). In the last 2 sessions, ADC values after fasting were $0.94 \pm 0.08 \times 10^{-3}$ mm^2/s and $0.93 \pm 0.07 \times 10^{-3}$ mm^2/s after a carbohydrate-rich meal (no statistically significant difference: $P = 0.45$) (Figs. 5, 6). Mean paired intraindividual differences between fasting and a protein- or carbohydrate-rich food intake were 10.5% (11.6%) and 9.8% (7.7%), respectively. We obtained similar mean (SD) paired intraindividual differences between the first session of fasting and the third session of fasting (11.8% [7.7%]). The calculated CVs for each participant and each session were similar to the ADC measurements for the intermediate b values (9.3%, 9.0%, 5.5%, and 6.0%, respectively). The overall CV for high b values was 7.5% (Table 2). The measured mean ADC values for high b values were significantly lower compared with the ADC values for intermediate b values for all measurements ($P < 0.001$).

Apparent Diffusion Coefficient Measurements Using a Monoexponential Model

The ADC values for each b value using a 2-point calculation (assuming a monoexponential model) are provided in Table 3. The mean ADC value for the monoexponential model for b values of 0 and 1000 s/mm^2 was $1.21 \pm 0.09 \times 10^{-3}$ mm^2/s, which was significantly higher compared with the ADC values from the fit to the high–b-values scheme by $0.28 \pm 0.12 \times 10^{-3}$ mm^2/s ($P < 0.01$).

Phantom Measurements

The phantom represented a model for water diffusion without perfusion effects. The DWI signal of the examined phantom showed a pure monoexponential dependence on the signal on the b value (Fig. 7), thereby confirming the validity of the applied DWI imaging protocol. Applying all acquired b values between b0 and b1000 for the monoexponential fitting algorithm, an ADC of $2.17 \pm 0.04 \times 10^{-3}$ mm^2/s was measured.

DISCUSSION

With this study, we demonstrate that the physiological postprandial changes in portal blood flow do not influence liver DWI and

TABLE 1. Measured ADC Values and Mean Difference Between Normalized Signal Curve and Mathematical Model

	ADC Intermediate b Values, 10^{-3} mm^2/s	Δ Difference to the Exponential Curve	ADC High b Values, 10^{-3} mm^2/s	Δ Difference to the Exponential Curve
Participant	Fasting/Protein	Fasting/Protein	Fasting/Protein	Fasting/Protein
1	1.4/1.4	0.0007/0.0097	1.0/0.8	0.0010/0.0027
2	1.3/1.1	0.0083/0.0043	0.8/1.0	0.0017/0.0073
3	1.2/1.0	0.0043/0.0093	0.9/0.9	0.0013/0.0010
4	1.4/1.2	0.0063/0.0003	1.0/0.9	0.0057/0.0003
5	1.0/1.5	0.0046/0.0093	0.7/0.8	0.0067/0.0000
6	1.6/1.9	0.0093/0.0067	0.7/0.7	0.0060/0.0013
7	1.1/1.1	0.0067/0.0033	0.8/0.9	0.0053/0.0047
8	1.2/1.4	0.0033/0.0073	0.9/0.9	0.0017/0.0053
9	1.2/1.6	0.0010/0.0063	1.0/1.1	0.0033/0.0057
10	1.3/1.2	0.0020/0.0063	1.0/0.9	0.0003/0.0060
Mean	1.3/1.4	0.0047/0.0062	0.9/0.9	0.0033/0.0034
SD	0.2/0.3	0.0029/0.0031	0.1/0.1	0.0024/0.0027

ADC indicates apparent diffusion coefficient.

the corresponding ADC values. The intraindividual ADC differences between fasting and food intake are in the order of 10% or less. According to these findings, a special preparation of patients regarding food intake before liver DWI is not necessary. Moreover, we are able to show that liver DWI is a robust technique with little intraindividual variability. A further finding of this study is that liver DWI follows a triexponential signal decay, which confirms the measurements of a previous study from Hayashi et al.[18]

A substantial increase in the portal venous flow was found 30 minutes after food intake. It has been previously reported that the increase in the portal blood flow is maximal at approximately 30 to 45 minutes after food intake.[39,40] We applied both, a protein- and carbohydrate-rich meal, respectively, because previous studies demonstrated an important role of different food components. Compared with protein-rich food, the increase in the portal volume was significantly higher after ingestion of carbohydrate-rich food. These results are in good concordance with previously published studies.[41–43]

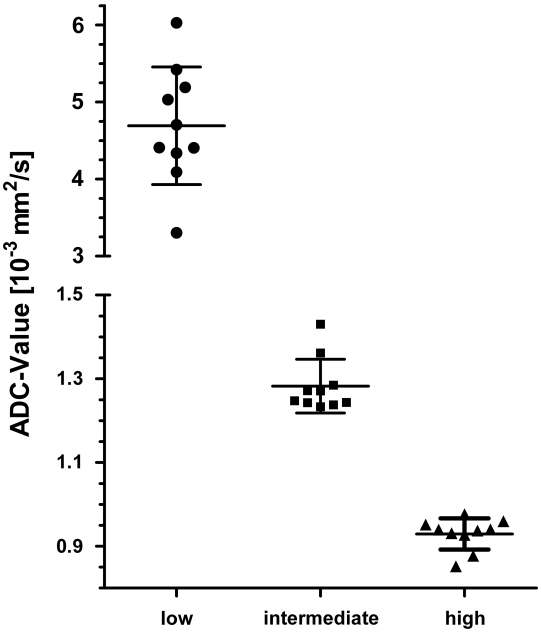

FIGURE 5. Dot plot of mean ADC values for each of the 10 study participants across all ROI measurements and sessions for low b values (dots), intermediate b values (squares), and high b values (triangles). The solid lines indicate the mean (SD) values. Note that the interindividual variation is substantially higher for low b values than for intermediate and high b values.

The image quality of the DWI protocol is essential to assure robustness. In our study, a single spin-echo echo-planar sequence was applied during shallow free breathing in combination with a sensitivity encoding parallel imaging acceleration technique to reduce the TE, which was reported to provide liver diffusion images with higher image quality and improved signal-to-noise ratio compared with breath-hold techniques.[44,45] To allow for complete coverage of the liver volume within practicable measurement time and to avoid potential pseudo–anisotropy artifacts,[46] a respiratory triggering technique, for example, using a breathing-belt or navigator-triggering technique, was not applied. Respiratory-triggered liver DWI was demonstrated to be less reproducible compared with free-breathing techniques.[45] Moreover, breath-hold echo-planar imaging sequences were reported to be more sensitive to cardiac and bowel motion.[47]

In a previous study, Hollingsworth et al[48] measured higher postprandial ADC values in the anterior right lobe at high b values (500 and 750 s/mm^2) and at b = 200 s/mm^2; they found a significant increase of ADC in both anterior and posterior right lobes. These results seem to be partly in contradiction to our measurements. However, they used a monoexponential calculation of ADC values including the b = 0 value, which, as we were able to show, overestimates true water diffusion including fast-moving spin ensembles from flow and perfusion effects. However, even when using low and intermediate b values, we did not find a measurable change of the ADC value after food intake.

The ADC values for high b values found in our study are lower than the measured ADC values from most previously reported studies at 1.5 T.[16,17] These studies used slightly different sequence parameters, acquisition protocols, and a different set of b values. However, the main difference seems to lie in the postprocessing for the ADC quantification. These previous studies calculated ADC values and diffusion maps using the intravoxel incoherent motion theory, which allows the separate calculation of perfusion and diffusion, on the basis of the assumption of a biexponential behavior of the signal.[16,17,23] In our study, the diffusion-related signal decay could be

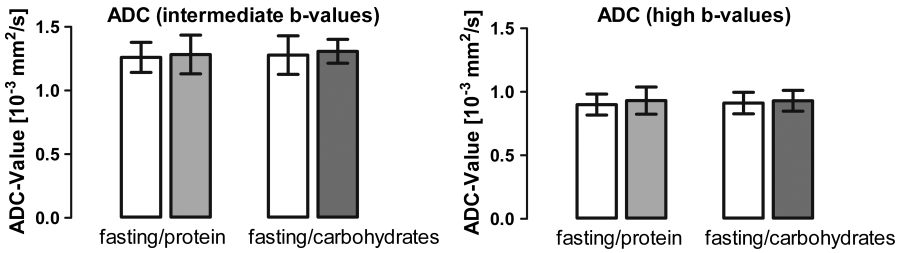

FIGURE 6. Comparison of the measured ADC values of the right liver lobe of the healthy study participants (n = 10) after fasting for at least 8 hours and after a protein- or carbohydrate-rich meal using intermediate b values (b50, b150, and b250 s/mm^2; left graph) and high b values (b500, b750, and b1000 s/mm^2; right graph).

well described by a triexponential approach, which was recently reported by Hayashi et al[18] as well. We interpreted the different components as microscopic motion of water with different velocity. We hypothesized that using low b values (b0-b50 s/mm^2) predominantly measures the blood flow of small vessels (venules), whereas intermediate b values (b values in our study: b50, b150, and b250 s/mm^2) potentially correspond to sinusoidal blood perfusion. The monoexponential signal decay observed for high b values (>b500 s/mm^2) presumably only reflects "pure" water diffusion. In our postprocessing algorithm, a separate fit for each b-value scheme was performed (low, intermediate, high b values) instead of only 1 triexponential fit to the signal curve, which was motivated by the fact that such a triexponential fit typically shows only little stability regarding the starting values for the fit because of the high number of fitting variables, which would be a prerequisite for meaningful computation of diffusion parameters. Because the ADC values for the different aspects of diffusion were separated in a previous study,[18] our approach seems justified because this indicates that the error introduced by separate fitting is negligible. We were able to confirm this by showing that the separate fitting of each phase results in an error of the fitting curve of less than 0.5% from the measurement points while providing stable results. Still, this approach may have disadvantages such as overfitting for instance. Further studies may want to investigate the best-suited model for fitting such data. A possibility would be to use an information criterion (for instance, the Bayes information criterion) to select the best-suited model. However, this was beyond the scope of this study.

Even when using low and intermediate b values, we did not detect changes in mean ADC values despite significantly increased portal vein flow. One explanation for this could be that the hepatic microcirculation is under the control of an intrinsic mechanism called *hepatic arterial buffer response*, which serves to maintain the liver perfusion as constant as possible.[49–51] Furthermore, many hormonal, neural, and metabolic mechanisms affect the hepatic microcirculation.[51–53] Therefore, the parenchymal liver perfusion seems predominantly unaffected by the increased portal venous flow. However, we cannot exclude the fact that using b values lower than 50 s/mm^2 potentially allows for detection of a significant influence of the portal venous flow caused by spin components with high flow velocity, which might not be detectable at b = 50 s/mm^2 and that requires even lower b values.

Using the interpretation described previously, our results are in good accordance to previous data. Perman et al[54] omitted the b0 image to minimize the influence of the liver perfusion on the ADC calculation and obtained ADC values similar to our measurements (0.98×10^{-3} mm^2/s). Studies, which included intermediate b values, reported higher ADC[4,6,7] because of the influence of the liver microcirculation on b values lower than 200 s/mm^2. Braithwaite et al[13] performed liver DWI on healthy volunteers in free breathing. They showed that different ROI measurements within the right hepatic lobe do not have relevant effects on ADC measurements with a measured CV of 12.8% of the liver ADC. Our results confirm this intraindividual stability of liver ADC values at 1.5 T (we detected CV of 7.2% for intermediate b values and 7.5% for high b values).

Our study has the following limitations:

1) To avoid cardiac motion-related artifacts, we evaluated only the right hepatic lobe. The limitation of the measurement time did not allow for cardiac gating.
2) Only protein- and carbohydrate-rich food was used. Previous studies have demonstrated an important role of different food components in terms of liver perfusion, including fat. We cannot exclude a potential effect of fat-rich food, which was reported to induce the greatest increase in postprandial portal blood flow.[41–43]
3) We measured the blood flow in the portal vein; however, we did not measure the entire hepatic microcirculation (including arterial supply) with a reference method such as $^{15}OH_2$ water positron emission tomography because this would have been out of the scope of this study.
4) Our results were obtained at 1.5 T only. Three-tesla MRI is increasingly used in clinical practice for abdominal imaging. As previously

TABLE 2. Comparison of the CV of Liver ADC Measurements of Intermediate With High b Values Within the Different Imaging Sessions

CV of Liver ADC Measurements, %	Session 1	Session 2	Session 3	Session 4	Overall
Intermediate b values	9.3	9.0	5.5	6.1	7.5
High b values	8.2	7.2	7.8	5.7	7.2

ADC indicates apparent diffusion coefficient; CV, coefficients of variation.

TABLE 3. Calculated ADC Values Using a 2-Point Calculation (b0 and b50–1000) Assuming a Monoexponential Model

b Value	Fasting	30 Min After Protein Intake	Fasting	30 Min After Carbohydrate Intake
50	4.70 (0.80)	4.79 (1.00)	4.67 (0.99)	4.66 (0.80)
150	2.50 (0.43)	2.50 (0.33)	2.74 (0.55)	2.58 (0.27)
250	1.97 (0.29)	2.00 (0.24)	2.02 (0.37)	1.96 (0.17)
500	1.54 (0.12)	1.53 (0.14)	1.53 (0.19)	1.55 (0.10)
750	1.34 (0.09)	1.36 (0.10)	1.35 (0.16)	1.39 (0.14)
1000	1.25 (0.12)	1.24 (0.11)	1.24 (0.13)	1.24 (0.07)

All values are expressed as mean (SD).
ADC indicates apparent diffusion coefficient.

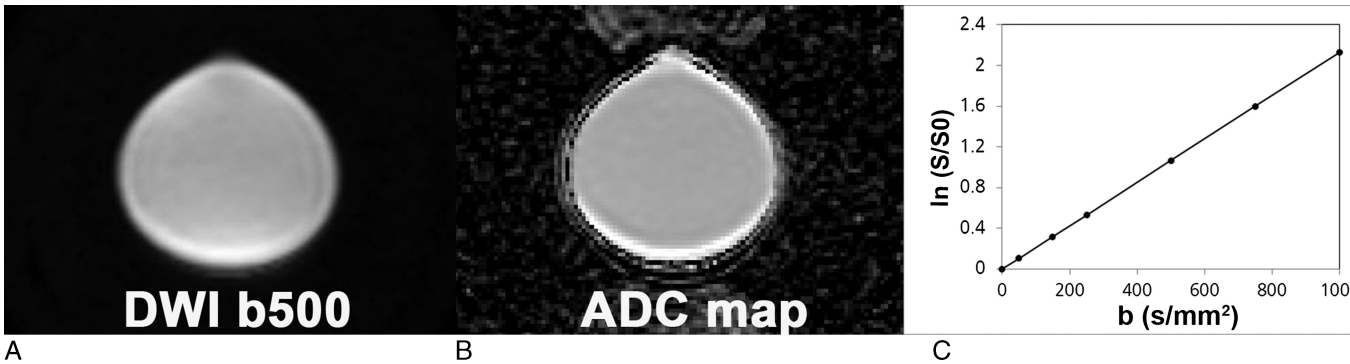

A B C

FIGURE 7. Water phantom scan: diffusion-weighted image at b = 500 s/mm2 (A) and corresponding ADC map (B) calculated using all b values (b0, b50, b150, b250, b500, b750, b1000 s/mm^2). C, Logarithmic plot of the monoexponential decay observed in the phantom examination representing pure water diffusion.

reported, measured liver ADC values may depend on the field strength.[54,55]

5) We evaluated only a cohort of healthy volunteers without history of liver disease. Therefore, we neglected the assessment of liver fibrosis or liver fat content, which, in principle, could be measured as well with MRI.[56,57]

In summary, we demonstrated that the physiological postprandial increase of the portal flow rate is not reflected in changes of water diffusion in liver parenchyma measured by series of b-values greater than 50 s/mm^2. Diffusion-weighted imaging and quantitative ADC values are highly robust across fasting and postprandial states, thus obviating the need for prescan food-intake precautions.

REFERENCES

1. Girometti R, Furlan A, Esposito G, et al. Relevance of b-values in evaluating liver fibrosis: a study in healthy and cirrhotic subjects healthy liver using two single-shot spin-echo echo-planar diffusion-weighted sequences. *J Magn Reson Imaging*. 2008; 28:411–419.
2. Muller MF, Prasad P, Siewert B, et al. Abdominal diffusion mapping with use of a whole body echo-planar system. *Radiology.* 1994;190:475–478.
3. Fujimoto K, Tonan T, Azuma S, et al. Evaluation of the mean and entropy of apparent diffusion coefficient values in chronic hepatitis C: correlation with pathologic fibrosis stage and inflammatory activity grade. *Radiology.* 2011;258: 739–748.
4. Taouli B, Tolia AJ, Losada M, et al. Diffusion-weighted MRI for quantification of liver fibrosis: preliminary experience. *AJR Am J Roentgenol*. 2007;189:799–806.
5. Parikh T, Drew SJ, Lee VS, et al. Focal liver lesion detection and characterization with diffusion-weighted MR imaging: comparison with standard breath-hold T2-weighted imaging. *Radiology.* 2008;246:812–822.
6. Taouli B, Vilgrain VR, Dumont E, et al. Evaluation of liver diffusion isotropy and characterization of focal hepatic lesions with two single-shot echo-planar MR imaging sequences: prospective study in 66 patients. *Radiology.* 2003;226:71–78.
7. Yamada I, Aung W, Himeno Y, et al. Diffusion coefficients in abdominal organs and hepatic lesions: evaluation with intravoxel incoherent motion echo-planar MR imaging. *Radiology.* 1999;210:617–623.
8. Agnello F, Ronot M, Valla DC, et al. High-b-value diffusion-weighted MR imaging of benign hepatocellular lesions: quantitative and qualitative analysis. *Radiology.* 2012;262:511–519.
9. Marugami N, Tanaka T, Kitano S, et al. Early detection of therapeutic response to hepatic arterial infusion chemotherapy of liver metastases from colorectal cancer using diffusion-weighted MR imaging. *Cardiovasc Intervent Radiol*. 2009;32:638–646.
10. Cui Y, Zhang XP, Sun YS, et al. Apparent diffusion coefficient: potential imaging biomarker for prediction and early detection of response to chemotherapy in hepatic metastases. *Radiology.* 2008;248:894–900.
11. Bonekamp S, Jolepalem P, Lazo M, et al. Hepatocellular carcinoma: response to TACE assessed with semiautomated volumetric and functional analysis of diffusion-weighted and contrast-enhanced MR imaging data. *Radiology.* 2011;260:752–761.
12. Thoeny HC, et al. Effect of vascular targeting agent in rat tumor model: dynamic contrast-enhanced versus diffusion-weighted MR imaging. *Radiology.* 2005;237:492–499.
13. Braithwaite AC, Dale BM, Boll DT, et al. Short- and midterm reproducibility of apparent diffusion coefficient measurements at 3.0-T diffusion-weighted imaging of the abdomen. *Radiology.* 2009;250:459–465.
14. Colagrande S, Pasquinelli F, Mazzoni LN, et al. MR-diffusion weighted imaging of healthy liver parenchyma: repeatability and reproducibility of apparent diffusion coefficient measurement. *J Magn Reson Imaging*. 2010;31:912–920.
15. Bilgili MY. Reproductibility of apparent diffusion coefficients measurements in diffusion-weighted MRI of the abdomen with different b values. *Eur J Radiol*. 2012;81:2066–2068.
16. Luciani A, Vignaud A, Cavet M, et al. Liver cirrhosis: intravoxel incoherent motion MR imaging—pilot study. *Radiology.* 2008;249:891–899.
17. Dijkstra H, Baron P, Kappert P, et al. Effects of microperfusion in hepatic diffusion weighted imaging. *Eur Radiol*. 2012;22:891–899.
18. Hayashi T, Miyati T, Takahashi J, et al. Diffusion analysis with triexponential function in liver cirrhosis. *Radiol Phys Technol*. 2013. [Epub ahead of print].
19. Chiaradia M, Baranes L, Pigneur F, et al. Liver magnetic resonance diffusion weighted imaging: 2011 update. *Clin Res Hepatol Gastroenterol*. 2011;35:539–548.
20. Takahara T, Kwee TC, Van Leeuwen MS, et al. Diffusion-weighted magnetic resonance imaging of the liver using tracking only navigator echo: feasibility study. *Invest Radiol*. 2010;45:57–63.
21. Dale BM, Braithwaite AC, Boll DT, et al. Field strength and diffusion encoding technique affect the apparent diffusion coefficient measurements in diffusion-weighted imaging of the abdomen. *Invest Radiol*. 2010;45:104–108.
22. Annet L, Peeters F, Abarca-Quinones J, et al. Assessment of diffusion-weighted MR imaging in liver fibrosis. *J Magn Reson Imaging*. 2007;25:122–128.
23. Le Bihan D, Breton E, Lallemand D, et al. MR imaging of intravoxel incoherent motions: application to diffusion and perfusion in neurologic disorders. *Radiology.* 1986;161:401–407.
24. Le Bihan D, Breton E, Lallemand D, et al. Separation of diffusion and perfusion in intravoxel incoherent motion MR imaging. *Radiology.* 1988;168:497–505.
25. Patel J, et al. Diagnosis of cirrhosis with intravoxel incoherent motion diffusion MRI and dynamic contrast-enhanced MRI alone and in combination: preliminary experience. *J Magn Reson Imaging*. 2010;31:589–600.
26. Moteki T, Horikoshi H. Evaluation of noncirrhotic hepatic parenchyma with and without significant portal vein stenosis using diffusion-weighted echo-planar MR on the basis of multiple-perfusion-components theory. *Magn Reson Imaging*. 2011;29:64–73.
27. Koh DM, Collins DJ, Orton MR. Intravoxel incoherent motion in body diffusion-weighted MRI: reality and challenges. *AJR Am J Roentgenol*. 2011; 196:1351–1361.
28. Sadek AG, Mohamed FB, Outwater EK, et al. Respiratory and postprandial changes in portal flow rate: assessment by phase contrast MR imaging. *J Magn Reson Imaging*. 1996;6:90–93.
29. Svensson CK, Edwards DJ, Mauriello PM, et al. Effect of food on hepatic blood flow: implications in the food effect phenomenon. *Clin Pharmacol Ther.* 1983;34:316–323.
30. O'Brien S, Keogan M, Patchett S, et al. Postprandial changes in portal haemodynamics in patients with cirrhosis. *Gut*. 1992;33:364–367.
31. Gaiani S, Bolondi S, Bassi S, et al. Effect of meal on portal haemodynamics in healthy humans and in patients with chronic liver disease. *Hepatology.* 1989; 9:815–819.
32. Sieber C, Beglinger C, Jaeger K, et al. Regulation of postprandial mesenteric blood flow in humans: evidence for a cholinergic nervous reflex. *Gut*. 1991; 32:361–366.
33. Yzet T, Bouzerar R, Baledent O, et al. Dynamic measurements of total hepatic blood flow with phase contrast MRI. *Eur J Radiol*. 2010;73:119–124.

34. Yzet T, Bouzerar R, Allart JD, et al. Hepatic vascular flow measurements by phase contrast MRI and Doppler echography: a comparative and reproducibility study. *J Magn Reson Imaging*. 2010;31:579–588.
35. Nasu K, Kuroki Y, Fujii H, et al. Hepatic pseudo-anisotropy: a specific artefact in hepatic diffusion-weighted images obtained with respiratory triggering. *MAGMA*. 2007;20:205–211.
36. Mürtz P, Flacke S, Träber F, et al. Abdomen: diffusion-weighted MR imaging with pulse-triggered single-shot sequences. *Radiology.* 2002;224:258–264.
37. Kwee TC, Takahara T, Niwa T, et al. Influence of cardiac motion on diffusion-weighted magnetic resonance imaging of the liver. *MAGMA*. 2009;22:319–325.
38. cp. Čížek, Pavel (2004) : (Non) Linear Regression Modeling, Papers/Humboldt-Universität Berlin, Center for Applied Statistics and Economics (CASE), No. 2004,11, http://hdl.handle.net/10419/22185.
39. Iwao T, Toyonaga A, Oho K, et al. Postprandial splanchnic hemodynamic response in patients with cirrhosis of the liver: evaluation with "triple-vessel" duplex US. *Radiology.* 1996;201:711–715.
40. Salo S, Alanen A, Komu M, et al. Effect of fasting and food intake on magnetization transfer of human liver tissue. *Magn Reson Imaging*. 1997;15:47–50.
41. Siregar H, Chou CC. Relative contribution of fat, protein, carbohydrate, and ethanol to intestinal hyperemia. *Am J Physiol*. 1982;242:G27–G31.
42. Sieber C, Beglinger C, Jäger K, Stalder GA. Intestinal phase of superior mesenteric artery blood flow in man. *Gut*. 1992;33:497–501.
43. Qamar MI, Read AE. Effects of ingestion of carbohydrate, fat, protein, and water on the mesenteric blood flow in man. *Scand J Gastroenterol*. 1988; 23:26–30.
44. Kandpal H, Sharma R, Madhusudhan KS, et al. Respiratory-triggered versus breath-hold diffusion-weighted MRI of liver lesions: comparison of image quality and apparent diffusion coefficient values. *AJR Am J Roentgenol*. 2009; 192:915–922.
45. Kwee TC, Takahara T, Koh DM, et al. Comparison and reproducibility of ADC measurements in breathhold, respiratory triggered, and free-breathing diffusion-weighted MR imaging of the liver. *J Magn Reson Imaging*. 2008;28:1141–1148.
46. Nasu K, Kuroki Y, Sekiguchi R, et al. Measurement of the apparent diffusion coefficient in the liver: is it a reliable index for hepatic disease diagnosis? *Radiat Med*. 2006;24:438–444.
47. Koh DM, Collins DJ. Diffusion-weighted MRI in the body: applications and challenges in oncology. *AJR Am J Roentgenol*. 2007;188:1622–1635.
48. Hollingsworth KG, Lomas DJ. Influence of perfusion on hepatic MR diffusion measurement. *NMR Biomed*. 2006;19:231–235.
49. Lautt WW. Relationship between hepatic blood flow and overall metabolism: the hepatic arterial buffer response. *Fed Proc*. 1983;42:1662–1666.
50. Lautt WW, Greenway CV. Conceptual review of the hepatic vascular bed. *Hepatology.* 1987;7:952–963.
51. Blankenship LL Jr, Cilento EV, Reilly FD. Hepatic microvascular regulatory mechanisms. XI. Effects of serotonin on intralobular perfusion and volumetric flowrates at the inlet of periportal and outlet of centrivenous sinusoids. *Microcirc Endothelium Lymphatics*. 1991;7:57–75.
52. Greenway CV, Stark RD. Hepatic vascular bed. *Physiol Rev.* 1971;51:23–65.
53. Reilly FD, McCuskey RS, Cilento EV. Hepatic microvascular regulatory mechanisms. I. Adrenergic mechanisms. *Microvasc Res*. 1981;21:103–116.
54. Perman WH, Balci NC, Akduman I, et al. Magnetic resonance measurement of diffusion in the abdomen. *Top Magn Reson Imaging*. 2009;20:99–104.
55. van den Bos IC, Hussain SM, Krestin GP, et al. Liver imaging at 3.0 T: diffusion-induced black-blood echo-planar imaging with large anatomic volumetric coverage as an alternative for specific absorption rate-intensive echo-train spin-echo sequences: feasibility study. *Radiology.* 2008;248:264–271.
56. Kang BK, Yu ES, Lee SS, et al. Hepatic fat quantification: a prospective comparison of magnetic resonance spectroscopy and analysis methods for chemical-shift gradient echo magnetic resonance imaging with histologic assessment as the reference standard. *Invest Radiol*. 2012;47:368–375.
57. Kuhn JP, Evert M, Friedrich N, et al. Noninvasive quantification of hepatic fat content using three-echo dixon magnetic resonance imaging with correction for T2* relaxation effects. *Invest Radiol*. 2011;46:783–789.